I&EC research
Industrial & Engineering Chemistry Research
pubs.acs.org/IECR
Article

Multiobjective Optimal Controlled Variable Selection for a Gas Turbine–Solid Oxide Fuel Cell System Using a Multiagent Optimization Platform

Temitayo Bankole, Debangsu Bhattacharyya,* Paolo Pezzini, Berhane Gebreslassie, Nor Farida Harun, David Tucker, Urmila Diwekar, and Kenneth M. Bryden

Cite This: *Ind. Eng. Chem. Res.* 2020, 59, 20058–20070
Read Online
ACCESS | Metrics & More | Article Recommendations

ABSTRACT: Hybrid gas turbine–fuel cell systems have immense potential for high efficiency in electrical power generation with cleaner emissions compared with fossil-fueled power generation. A systematic controlled variable (CV) selection method is deployed for a hybrid gas turbine–fuel cell system in the HyPer (hybrid performance) facility at the U.S. Department of Energy's National Energy Technology Laboratory (NETL) for maximizing its economic and control performance. A three-stage approach is used for the CV selection comprising a priori analysis, multiobjective optimization, and a posteriori analysis. The a priori analysis helps to screen off several candidate CVs, thus reducing the size of the combinatorial optimization problem for multiobjective CV selection. For optimal CV selection, a transfer function model of the HyPer facility is identified. By considering several candidate models, the final transfer function model is selected using Akaike's Final Prediction Error criterion. Experimental data from the HyPer facility are used to estimate the noise in the measurement data. For solving the combinatorial multiobjective optimization problem for CV selection, a multiagent optimization platform comprising simulated annealing, genetic algorithm, and efficient ant colony optimization algorithms is used. Pareto-optimal CV sets exhibit a high trade-off between the economic and control objective. The a posteriori analysis is undertaken for several top Pareto-optimal CV sets. An optimal CV set is selected that shows the best compromise between process economics and controllability under both nominal and off-design conditions.

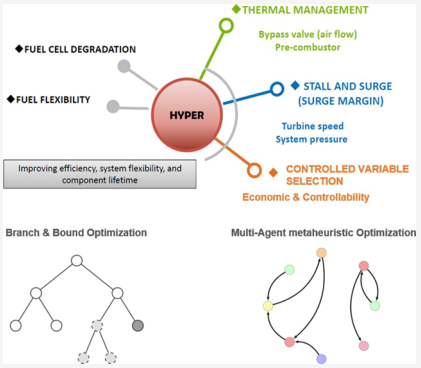

1. INTRODUCTION

In the quest for highly efficient and cleaner power production systems, various advanced power cycles are being investigated. One such system is the gas turbine (GT)–solid oxide fuel cell (SOFC) hybrid system where a GT is synergistically coupled with an SOFC. SOFCs[1] are small-dimensional, stationary, high-temperature, low-noise power generation devices with immense potential to replace currently used combustion-based power generation systems. SOFCs mainly consist of an anode, a cathode, and a solid oxide electrolyte sandwiched in between. While fuel is fed to the anode, air is fed to the cathode side. These electrodes are connected externally by an electrical circuit. Extensive details on modeling of SOFC systems can be found in the literature.[2,3]

The GT-SOFC system promises very high theoretical energy efficiencies when compared with other systems.[4,5] They can be considered as part of the polygeneration systems where integration of multiple processes are considered for coproducing multiple products such as heat, power, and chemicals. These systems enable system flexibility and efficient resource utilization. By feeding the fuel cell hybrid systems with the syngas from the coal-fed integrated gasification-combined cycle power systems, advanced coal-based power generation with higher efficiency and cleaner emission can be accomplished.[5] Fuel cell hybrid systems are not only attractive for stationary applications but also for mobile systems such as ships and aircrafts.

While high efficiency is desired for maximizing the economic performance of the GT-SOFC system, sufficient controllability must be ensured for this challenging system. While compressor surge must be prevented, fluctuations in temperature of the inlet air to the SOFC must be minimized as this can cause dramatic degradation in the fuel cell due to thermal stress. Therefore, optimal selection of controlled variables (CVs) for this system with due consideration of trade-offs between the

Received: June 10, 2020
Revised: October 9, 2020
Accepted: October 16, 2020
Published: November 2, 2020

https://dx.doi.org/10.1021/acs.iecr.0c02865
Ind. Eng. Chem. Res. 2020, 59, 20058–20070

economic and control performance would be an important step toward commercialization of this technology.

Optimal selection of the primary CVs is one of the most important aspects of control structure design.[6] CV selection is focused on selecting optimal variables to be controlled, rather than how to control these variables. Importance of the optimal CV selection has been discussed in detail in a number of reviews on control structure design.[7−9]

Typically, CV selection has been done following process heuristics.[10,11] There are three main issues with these heuristic-based approaches. First, these heuristics cannot be applied to novel processes for which there is lack of process knowledge or experience such as the GT-SOFC systems. Even if the entire process is not novel, but if only a section or an equipment item as part of a plant is replaced or modified, re-evaluation of the CV sets is desired. For example, if only the fuel cell is replaced by a different technology in the hybrid system, optimal CVs can be different. Second, the CVs selected based on heuristics do not necessarily ensure that both the process economics and controllability are maximized especially in the face of disturbances. Third, the economic objective for process control and/or process operating constraints can change with time. This can lead to a change in the optimal CVs. However, optimal selection of CVs by evaluating all possible combinations of candidate CVs may be challenging for systems where there are a large number of candidate CVs. Therefore, not only a systematic approach to CV selection is desired, but also it is desired that the CV selection algorithm can be solved within some reasonable amount of time for systems with a large number of possible combinations of CV sets.

A number of properties are desired for the optimal CVs. If the setpoints of the CVs remain fixed at the predetermined setpoints irrespective of changes in disturbances, then it will be desired that the selected CV sets result in minimal loss from the optimal operation (loss here is defined as the difference between the optimal value of the operational objective function and its value when the CVs are kept at the predetermined setpoints). This is known as the self-optimizing property.[12] In addition, the CVs should possess the following properties:

- Low sensitivity to disturbances
- Ease of measurement and control

A systematic approach to obtaining optimal CVs has been proposed by Skogestad.[12] The approach was further modified[13] by proposing a three-stage procedure: a priori analysis, CV selection, and a posteriori analysis. In the a priori analysis, prescreening criteria are applied to eliminate CVs that would result in a poor servo or regulatory control performance. Candidate CVs obtained from the a priori analysis are evaluated at the second stage for selecting the optimal CV set(s). At this stage, if only a measure of process economics is considered as the objective for CV selection, it can lead to infeasible and/or uncontrollable CV sets. The authors[13] proposed incorporating measures of controllability, loop interaction, and dead time along with process economics in the CV selection algorithm. Finally, in the last step, the obtained candidate CVs are examined in the a posteriori analysis to evaluate the controllability and/or economic performance under off-design conditions.

The major computational expense in the CV selection problem is in the second stage, where the combinatorial optimization problem is solved. This stage seeks to find the Pareto-optimal solution by considering the trade-off between the economic and control performances. For maximizing economic performance in the face of disturbances, typically self-optimizing performance of the CV sets is maximized.[14−16] In addition, the selected CV sets should satisfy some desired levels of controllability. For maximizing the controllability, the minimum singular value of the appropriately scaled gain matrix is maximized.[13] Time delay and loop interaction using relative gain array analysis are used as constraints in the optimization. The combinatorial optimization problem is typically solved using the branch and bound algorithm. One of the efficient algorithms in the literature is a bidirectional branch and bound algorithm, which is complete, nonredundant, and exhaustive.[15−17] However, for large-scale systems that suffer from combinatorial explosion of possibilities, the bidirectional branch and bound algorithm can take long time to solve the combinatorial optimization problem. While the CV selection algorithm is executed offline, it is desired that the algorithm be executed fast especially for systems where the algorithm needs to be executed frequently. The CV selection algorithm should be re-executed under several scenarios. First, it needs to be executed if the process and/or disturbance model changes and/or a list of CVs, MVs: manipulated variables, and/or DVs: disturbance variables change or their bounds change due to addition or removal of equipment items, including control elements, and/or addition or removal of measurements, and/or changes in the plant operating conditions. Second, the CV selection algorithm needs to be re-executed if the operational objective of the process plant changes. In this work, an approach that employs metaheuristic algorithms in a multi-agent[18] is considered for solving the combinatorial optimization problem. The main advantage of the multiagent techniques is the exploration and exploitation principle of metaheuristic algorithms where a solution space is continuously explored and the current best solutions are exploited to further search the feasible region for better solutions than the incumbent.[19] The technique consists of separate independent agents, which are coordinated by a master agent. These agents share solutions and learn from one another at the end of every iteration, which leads to faster convergence in comparison with the traditional techniques in literature.

While the CV selection algorithms have been applied to various chemical systems, to the best of our knowledge, there is no work in the literature on the optimal CV selection for the GT-SOFC system. The specific GT-SOFC system that is investigated here is the HyPer (hybrid performance) facility at the U.S. Department of Energy's National Energy Technology Laboratory (NETL) in Morgantown, West Virginia, USA.[4] Despite several studies on the dynamics of the HyPer facility and its interaction with the hardware,[4,5,20−22] the CVs for this process are currently selected heuristically. The HyPer facility is a cyber-physical system[23,24] where a software model is used for representing the SOFC. In this system, the cyber component can be modified or replaced or can be arranged in different configurations with the existing physical components and can be used for representing novel power cycle configurations.

It should be noted that the primary CV selection step is part of the top stage of the control system design approach.[13,14] This step is followed by the secondary CV selection[25] and then the control system design that involves decision about decentralized versus centralized controllers followed by the design of the controllers. Once the design of the entire control

https://dx.doi.org/10.1021/acs.iecr.0c02865
Ind. Eng. Chem. Res. 2020, 59, 20058−20070

system is completed, then its performance can be evaluated by performing transient studies.

2. OVERVIEW OF CONTROLLED VARIABLE SELECTION

The proposed methodology of designing a control structure for a complete chemical plant follows a rigorous approach as detailed.[13] There are three stages in this approach—a priori analysis, selection of the Pareto-optimal CV sets, and lastly, a posteriori analysis.

2.1. A Priori Analysis. The goal of the a priori analysis is formulation of the objective function, identification of disturbances and manipulated variables and quantification of their bounds, identification of active constraints, and finally prescreening off of poor candidate CVs. First, an objective function J must be determined based on the operational objective of the process. The objective function is typically a cost function, a profit function, or a measure of plant efficiency that is desired to be optimized. This is chosen to benchmark the effect of selecting different sets of variables on the economics of the process. Next, constraints (mainly operational and regulatory), manipulated variables (degrees of freedom), and disturbances are identified. Optimization is performed with respect to the identified degrees of freedom and due consideration of the constraints. This optimization process is carried out under nominal conditions as well as under disturbances. These optimization studies yield a number of important information. First, information about the optimal variation of the input and output variables is obtained. This information is used to construct scaling matrices for outputs and inputs, given by eqs 1 and 2, respectively.

$$D_y = \mathrm{diag}(\max(|c^{\mathrm{nom}} - c^{\mathrm{d}}|)) \tag{1}$$

$$D_u = \mathrm{diag}(\max(|u^{\mathrm{nom}} - u^{\mathrm{d}}|)) \tag{2}$$

In eqs 1 and 2, the superscript "nom" and "d" denote the nominal and disturbance conditions, respectively, "c" represents the CVs, and "u" represents the MVs. These scaling matrices are used in the next stage where the optimization is formulated.

Second, these optimization studies yield information about the active constraints, if any. These constraints are active in all optimization studies while considering nominal and disturbance conditions. These active constraints must be selected as CVs. Suitable MVs are selected from the available list, so that these CVs can be maintained within tight bounds. If there are additional MVs that can be used as degrees of freedom, then additional CVs are selected. Selecting these additional CVs is the focus of the remainder of this article.

For selecting the additional CVs, first, a list of remaining candidate CVs is generated. From this list, prescreening criteria are used to eliminate some of variables in order to eliminate infeasible or poor CVs, thus reducing the size of the combinatorial optimization in the next step. These prescreening criteria can be user-dependent. Generally, it would be desired to eliminate the variables that exhibit weak servo performance and/or are strongly affected by disturbances. Let n_y, n_u, n_d represent dimensions of measurements, manipulated variables, and disturbances, respectively. For applying these criteria, a linear process model is obtained from the process under nominal conditions as shown in eq 3 with $G_p \in \mathbb{R}^{n_y \times n_u}$ as the process gain matrix and $G_d \in \mathbb{R}^{n_y \times n_d}$ as the disturbance gain matrix. These gain matrices are scaled such that all elements of inputs u, outputs y, and disturbances d have a maximum magnitude of 1 (eq 4). The prescreening criteria are mathematically stated in eqs 4−6. If the inequality in eq 5 is not satisfied, no input can control the output variable y_j within the bounds. In addition, the candidate CVs y_j that have high dead time, represented by $\kappa(u_i, y_j)$—beyond a threshold χ_j—with respect to the available manipulated variables u_i can also be prescreened off using eq 6. The prescreening step can reduce the initial list of candidate CVs significantly, thus decreasing the size of the combinatorial optimization in the following step.

$$y = G_p u + G_d d \tag{3}$$

$$\left\|(G_p)_i\right\|_\infty = 1 \quad \forall \ i \tag{4}$$

$$\left\|(G_p)_i\right\|_\infty \geq \|(G_d)_i\|_\infty \quad \forall \ i \tag{5}$$

$$\kappa(u_i, y_j) \leq \chi_j \tag{6}$$

2.2. Selection of the Pareto-Optimal CV Sets. If the optimal setpoints of the selected CVs are computed for nominal operating conditions, these precomputed optimal setpoints become suboptimal whenever disturbances change from the nominal point. Thus, CVs are sought such that whenever disturbances change, the deviation between the actual value of the objective function J and its optimal value is minimized. This deviation is denoted as a loss function (J_L) as given by eq 7.

$$J_L = J(c, d) - J_{\mathrm{opt}}(d) \tag{7}$$

In eq 7, $J(c, d)$ denotes the value of the operational objective function J when CVs "c" are kept constant, while $J_{\mathrm{opt}}(c, d)$ represents the optimal value of the operational objective function J in the face of the disturbance d. It should be noted that if d were nominal, then J_L would be zero. It is desired to select CVs that minimize J_L in the face of disturbances.

Two forms of loss functions have been proposed in the literature: a worst case loss function[14] and an average loss function.[26] The average loss function as given in eq 8 is considered in this work. As discussed,[26] the average loss function is superoptimal in the sense that it also minimizes the worst case loss function. For more details on the discussion of the average loss function and worst-case loss function, interested readers are referred to ref 26. The average loss function takes into account the magnitude of the expected disturbances, given by a diagonal matrix $M_d \in \mathbb{R}^{n_d \times n_d}$ that is constructed based on the magnitudes of disturbances as quantified during the a priori analysis. The average loss function includes the magnitude of the expected control or implementation error, given by the diagonal matrix $M_n \in \mathbb{R}^{n_y \times n_y}$ to capture the impact of poor control performance and/or measurement error. Since the design of controllers is done at a later stage, performance of the controllers is hard to quantify during control structure design. Measurement error can be estimated if plant operational data are available as shown later in this paper for this specific application. In the absence of any measurement data and knowledge of the expected control system performance, the matrix M_n can be constructed based on the conservatism that a user would like to exercise in the CV selection due to poor control system

https://dx.doi.org/10.1021/acs.iecr.0c02865
Ind. Eng. Chem. Res. 2020, 59, 20058−20070

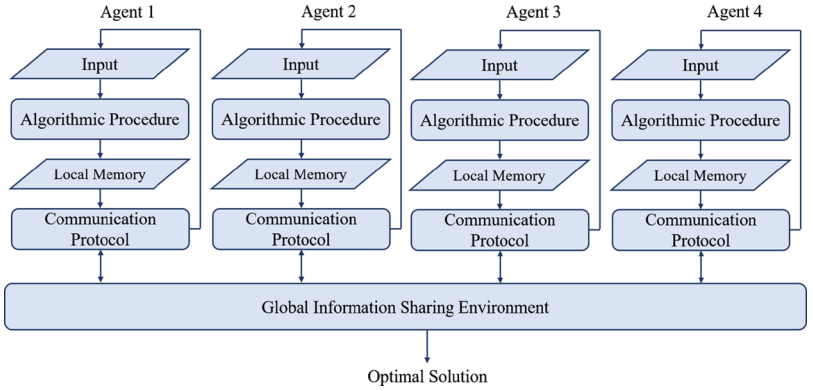

Figure 1. MAOP framework with four agents.

performance and measurement error.[1] In eq 8, $J_{uu} \in \mathbb{R}^{n_u \times n_u}$ represents the second order derivative of the cost function with inputs, while $J_{ud} \in \mathbb{R}^{n_u \times n_d}$ represents the second order derivative with respect to inputs and disturbances. The degree of freedom, that is, the number of manipulated variables, is denoted as n_u. The number of disturbances is denoted as n_d. The selection matrix $H \in \mathbb{R}^{n_u \times n_y}$ reduces the full gain matrix to the selected gain matrix of the chosen CV. For single variable selection, the matrix H must satisfy eq 9.

$$J_L = \frac{1}{6(n_u + n_d)} \left\| J_{uu}^{1/2} (HG_p)^{-1} (((HG_p) J_{uu}^{-1} J_{ud} - HG_d) M_d \quad HM_n) \right\|_F^2 \tag{8}$$

In eq 8, subscript "F" denotes the Frobenius norm. More details on the loss function and the derivation can be found.[14,13,26]

$$HH^T = I_{n_u} \tag{9}$$

In addition to minimizing loss in optimality of the objective function, the CVs must possess acceptable controllability. First, a scaled gain matrix $\hat{G}$ is generated as shown in eq 10 where it is scaled with respect to the optimal variation of the input and output variables as defined in eqs 1 and 2. The inverse of the minimum singular value of the scaled steady-state gain matrix is considered as the controllability function J_c as shown in eq 11. This represents the minimum gain from input to output for any input direction and is a measure of the difficulty in steering the process to a desired state using the available degrees of freedom.

$$\hat{G} = D_y^{-1} G_p D_u \tag{10}$$

$$J_c(c) = \underline{\sigma}^{-1}(\hat{G}) \tag{11}$$

The optimization problem is formulated as follows:

$$\min_H \{J_L(H), J_c(H)\}$$

Subject to

$$J_L(H) = \frac{1}{6(n_u + n_d)} \left\| J_{uu}^{1/2} (J_{uu}^{-1} J_{ud} - (\mathrm{HG})^{-1} HG_d) M_d \, J_{uu}^{1/2} (\mathrm{HG})^{-1} HM_n \right\|_F^2$$

$$J_c(H) = \underline{\sigma}^{-1}(H\hat{G})$$

$$\hat{G} = D_y^{-1} G_p D_u \tag{12}$$

While the proposed approach in this paper utilizes linear gain matrices around nominal points, the authors have a paper[27] in review for extending the CV selection to fully nonlinear models.

2.3. Optimization. For the optimal selection of additional primary CVs, a constrained multiobjective mixed integer nonlinear programming (MINLP) problem given by eq 12 is solved by evaluating the trade-off between the economic performance and controllability of the CVs. A parallelized multiobjective branch and bound algorithm was implemented[13] in order to solve the optimization defined in eq 12. This algorithm runs on a distributed computing server for computational efficiency; however, since this is completely exhaustive, this algorithm is inefficient for speedy enumeration of CV sets.

The multiagent optimization (MAOP) framework used in this paper uses a combination of different metaheuristic strategies (agents) such as the efficient ant colony,[28] simulated annealing,[29] and genetic algorithm.[30] The multiagent framework allows for the exploitation/combination of these methods and algorithms into a single framework, which further improves the speed of convergence (see Figures 1 and 2). This multiagent framework supports the cooperation of these individual agents predefined by protocols surrounding information sharing and exchange of data.

Each agent in the framework is designed to individually solve large-scale optimization problems.[31] Each agent/system possesses deterministic, stochastic, and heuristic algorithmic procedures. In the multiagent framework, each agent is defined by a set of distinct parameters, which include an algorithmic procedure, a communication protocol between the algorithmic procedure and the global information sharing environment, and the specific initialization procedure and solution retrieval mechanisms. The communication protocol determines the behavior of an agent and what type of information it shares with other agents. An agent in this sense is an autonomous and separate software entity that interacts with other members of the multiagent framework. The multiagent framework there-

https://dx.doi.org/10.1021/acs.iecr.0c02865
Ind. Eng. Chem. Res. 2020, 59, 20058−20070

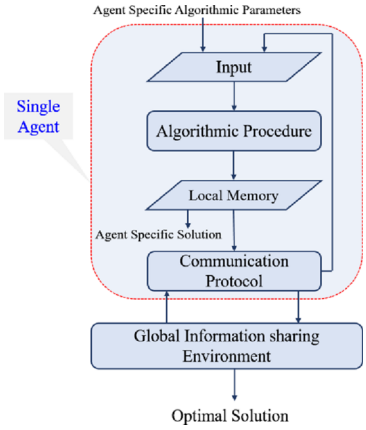

Figure 2. Agent in the MAOP framework.

fore exhibits the individual characteristics of the autonomous agents and the superior properties that arise from the interaction of the individual agents.

The multiagent framework includes the representation of the problem to be solved (including objective function and constraints), global sharing (that includes all local solutions from individual agents and solution metadata) memory environment, pool of algorithmic solvers, scheduler that allocates the resource and execution of the algorithmic agents to solve the tasks, and processing and retrieval of final solution. In contrast to conventional methods, the combination of several agents/algorithms in a pool allows for exploitation of the strengths of each algorithm. At the end of a preset number of iterations, the agents share the best results from their local memory with one another in the global information sharing environment, which allows the agents learn from one another, thus improving the speed of convergence to a global optimum. Additionally, should an agent become stuck at local optima, it can glean better results from other agents during this communication session. Readers are referred to ref 32 for a detailed discussion on the MAOP such as information sharing, global optimality, and convergence.

2.4. Posteriori Analysis. The a posteriori analysis entails evaluating the CV sets selected from the previous stage. This includes analysis of controllability under off-design conditions in order to evaluate CV sets that perform poorly. These CV sets are excluded as they would sacrifice process economics and controllability once the process departs from nominal conditions. It should be observed that minimization of the average loss given in eq 8 evaluates the economic performance across the values of the disturbances considered. However, it is pertinent to examine controllability as well.

3. GT-SOFC HYBRID SYSTEM

The GT-SOFC HyPer facility at the NETL has the capacity of reproducing power dynamcis of systems in a range of 300−900 kW. In this system, other than the single-shaft GT and a high-performance exhaust gas recuperator, several pressure vessels are used to capture the transeint effects of the physical volumes and flow resistances of the cyber-physical fuel cell, combustors, and its related chanelling and piping. The GT is an auxiliary power unit that is of Garrett Series 85 type and consists of a two-stage radial compressor. The HyPer facility utilizes two recuperators with countercurrent flow to preheat the air entering into the pressure vessel that faciliates to simulate the fuel cell cathode volume. The cyber system includes a real-time fuel cell model that is used to control the natural gas burner that simulates the thermal output of an SOFC. The real-time fuel cell model runs on a dSpace platform, which is generally used for hardware in the loop applications.

3.1. Process Description. The HyPer facility is as shown in Figure 3 and consists of a virtual fuel cell and the following subsystems:

1. Compressor/turbine model
2. Heat exchangers
3. Bypass valves

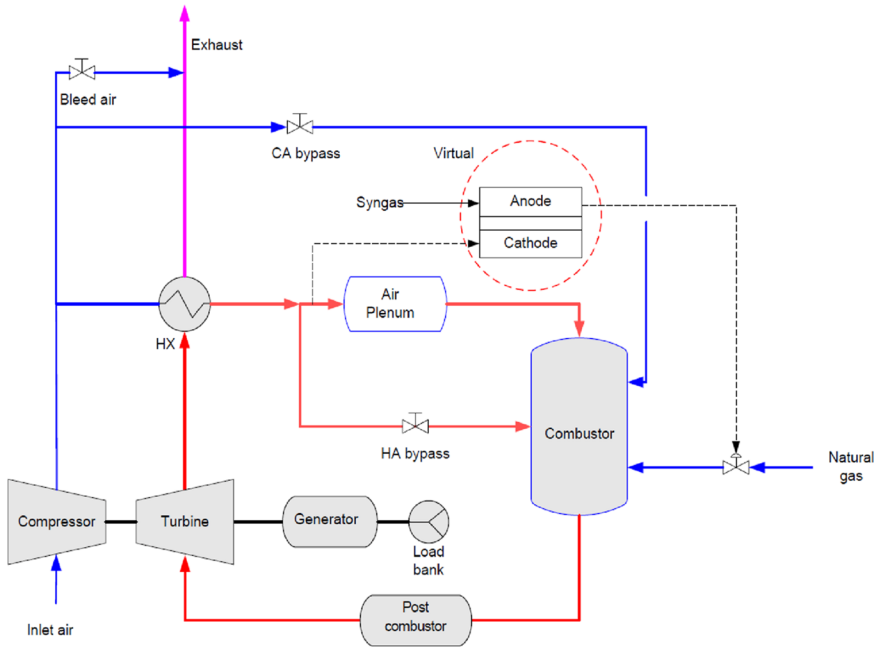

Figure 3. Configuration of the HyPer facility.

https://dx.doi.org/10.1021/acs.iecr.0c02865
Ind. Eng. Chem. Res. 2020, 59, 20058−20070

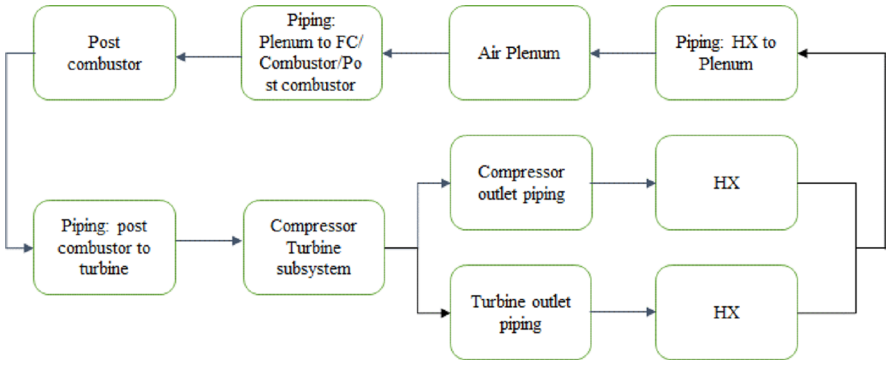

Figure 4. Simulink flowsheet for the HyPer facility.

4. Pressure vessels (an air plenum, a combustor, and a postcombustor)

The description of each subsystem is given in Sections 3.1.1 through 3.1.4. For brevity, all model equations for the subsystems are omitted here and can be found in ref 33.

3.1.1. Compressor/Turbine. This unit (auxiliary power unit) consists of a turbine and a compressor in a single-shaft assembly capable of producing 400 Hz of synchronous power. The compressor is a double-stage centrifugal compressor driven by the 120 kW turbine that is encased within the compressor scroll. The turbine nominally operates at 40,500 rpm. At this speed, approximately 2 kg/s of compressed air exits the compressor at a pressure ratio of 4.[34]

3.1.2. Heat Recuperation. The HyPer facility consists of a combustor and an air plenum that is used to reproduce the heat effluent and stack volume of the virtual 300 kW SOFC. The thermal efficiency of the facility is improved using heat exchangers (HX) to recover waste heat from the turbine exhaust to increase the temperature of the compressed air to the fuel cell stack. This closes the loop on the recuperated cycle.

For the purpose of heat recovery, two parallel counter-current heat exchangers are used. These primary heat recuperators transfer waste heat from the turbine exhaust to the compressed air before it enters the SOFC cathode. This significantly increases the temperature of the compressed air, thus reducing fuel requirements in the combustor. The typical effectiveness of the heat exchangers is 89% with cold-side and hot-side pressure losses of 2.5 and 3%, respectively. The maximum temperature for both sides is approximately 894 and 900 K for flows of about 1.83 and 1.77 kg/s, respectively.

3.1.3. Bypass Valves. The hardware configuration setup uses bypass valves within flow loops parallel to the mainstream flow pathways for the control of airflow to the air plenum. In order to minimize pressure losses in the system, no valves are used between the main pressure loop and the gas turbine. Currently, three parallel air flow control loops are being implemented in the HyPer facility, and these are the cold-air (CA) bypass valve, the bleed-air (BA) bypass valve, and finally, the hot-air (HA) bypass valve. These valves possess unique characteristics and attributes in controlling the system performance and efficiency. The bypass valves are used to mitigate the thermal management of the system and optimize the fuel cell−gas turbine performance during transient operations. The BA valve has also been shown to increase compressor discharge pressure and to increase stall margins. The HA valve on the other hand is effectively used to decrease cathode inlet flow. Additionally, it can lower the pressure drop by 10%. Lastly, the CA valve was shown to have a strong effect on the cathode airflow, decreasing the turbine inlet temperature and increasing the compressor surge margin.[4,35]

3.1.4. Pressure Vessels (Air Plenum, Combustor, and Postcombustor). The air plenum primarily serves as an SOFC volume and piping manifold. This pressure vessel is 2.0 m^3 in capacity. Similarly, the postcombustor as well as its associated piping is a pressure vessel with a volume of 0.78 m^3. These vessels are meant to simulate the residence time of the fuel cell either by use of metallic floats or apertures. The vessel as well as its channeling is created using 2.54 cm Incaloy 800AT and is intended to work at temperatures as high as 1200 K at a pressure of 310 kPag. It should be noted that the combustor simulates heat generation from the fuel cell and is controlled by fuel flow rates as seen in the virtual component of Figure 3. More details of the facility, piping, configuration, and process description can be found in ref 33. (see Figure 4 for flowsheet).

3.2. Setup of the CV Selection Problem. Figure 4 shows a flowsheet of how the model is laid out in Simulink, where each block represents a set of equations describing the subsystems, including equations for pressure drop calculations for flow through the piping network.

First, a list of candidate CVs and a list of available manipulated variables are enumerated as shown in Tables 1 and 2. The a priori analysis consists of prescreening off candidate CVs based on process insight and eqs 4−6. In the turbine/compressor subsection as shown in Figure 4, the turbine speed is a candidate CV and all other variables (including the pressure and temperature of the compressor and turbine exhaust) within this subsection are dependent on the turbine speed (due to the coupling of the turbine and compressor on the single-shaft assembly). The electric load is a disturbance and depends on the power demand of the grid (load bank for this specific example, see Figure 3). In the heat exchanger subsection, the available candidate CV is the temperature to the plenum. In the air plenum, the temperature is a candidate CV. Similarly, in the combustor subsystem, the temperature is a candidate CV. The mass flow rate to the postcombustor depends on the HA bypass, the CA bypass, and the mass flow rate to the plenum. The mass flow rate to the postcombustor and the mass flow rate to the plenum are both included as candidates; similarly, the temperature in the postcombustor is considered as a candidate. The initial sets of candidate CVs reduce from an initial list of 21 (Table 1) to 12 (Table 3) upon a priori analysis. This includes removal of CVs with poor controllability and high dead time according to eqs 5 and 6. The available degrees of freedom and disturbances are listed in Table 2.

https://dx.doi.org/10.1021/acs.iecr.0c02865
Ind. Eng. Chem. Res. 2020, 59, 20058−20070

Table 1. List of All Candidate CVs and their Respective Subsystem

s/n	subsystem	candidate CVs
1.	compressor/turbine subsystem	air mass flow rate to the compressor
2.		flue gas mass flow rate to the turbine
3.		compressor pressure
4.		compressor temperature
5.		turbine pressure
6.		turbine temperature
7.		turbine speed
8.	heat recuperation subsystem	temperature to the plenum
9.		exhaust turbine temperature
10.	pressure vessels (air plenum, combustor, postcombustor)	mass flow rate to the heat exchanger
11.		mass flow rate to the combustor
12.		air plenum temperature
13.		air plenum density
14.		air plenum pressure
15.		mass flow rate to the combustor
16.		combustor temperature
17.		mass flow rate to the postcombustor
18.		postcombustor temperature
19.		postcombustor pressure
20.		mass flow rate to the turbine
21.		temperature to the turbine

Table 2. List of Manipulated Variables and Disturbances

s/n	category	description
1.	manipulated variables	temperature from the turbine
2.		mass flow rate cold air
3.		mass flow rate hot air
4.		mass flow rate bleed air
5.	disturbances	fuel flow rate
6.		electric load

Table 3. Candidate CVs in the HyPer Facility

controlled variable	description
$\dot{m}_{\text{in, pl}}$	mass flow rate to the plenum
$T_{\text{in, pl}}$	temperature to the plenum
T_{pl}	temperature in the plenum
$T_{\text{in, turb}}$	inlet temperature to the turbine
T_{pc}	temperature in the postcombustor
T_{com}	temperature in the combustor
ω	turbine speed
$\dot{m}_{\text{in, HX}}$	mass flow rate to the heat exchanger
$\dot{m}_{\text{in, pc}}$	mass flow rate to the postcombustor
$\dot{m}_{\text{CA}}$	mass flow rate cold air
$\dot{m}_{\text{HA}}$	mass flow rate hot air
$\dot{m}_{\text{BA}}$	mass flow rate bleed air

3.2.1. Gain Matrices. In order to obtain the gain matrices as defined in eq 3, pseudo random binary sequence (PRBS) signals are designed for this multiple-input multiple-output system.[36] The design seeks to ensure persistence of excitation and statistical independence between the input(s) and disturbance(s). The frequency range of interest $[\bar{\omega}_*, \bar{\omega}^*]$ is given by

$$\bar{\omega}_* = \frac{1}{\beta_s \tau_{\text{dom}}^{\text{H}}} \leq \bar{\omega} \leq \frac{\alpha_s}{\tau_{\text{dom}}^{\text{L}}} = \bar{\omega}^* \tag{13}$$

where α_s is the fractional closed loop speed of the response of the process, β_s is an integer representing the number of time constants that correspond to the settling time that is defined in this work as the time taken by the output(s) to reach and stay within 5% of the final value. The fastest (lowest) dominant time constant is represented by $\tau_{\text{dom}}^{\text{H}}$, while the slowest (highest) dominant time constant is represented by $\tau_{\text{dom}}^{\text{L}}$. To ensure excitation in the desired frequency range, the switching time of the PRBS is calculated to satisfy eq 14.[36] Eq 15 is used to calculate the number of switches.

$$T_{\text{sw}} \leq \frac{2.8\tau_{\text{dom}}^{\text{L}}}{\alpha_s} \tag{14}$$

$$N_s^{(1)} = 2^{n_r} - 1 \geq \frac{2\pi\beta_s \tau_{\text{dom}}^{\text{H}}}{T_{\text{sw}}} \tag{15}$$

In eqs 14 and 15, n_r is the number of shift registers and T_{sw} is the switching time. The PRBS sequence is repeated after $N_s T_{\text{sw}}$ time units. The parameters α_s and β_s are specified to be 2.0 and 3.0, respectively. The PRBS is designed with the following parameters estimated from open loop tests: $\tau_{\text{dom}}^{\text{L}}$ = 50 s and $\tau_{\text{dom}}^{\text{H}}$ = 150 s. The input−output data are divided into model calibration and validation data.

The nominal values of the steady-state operating conditions were obtained[33] as 13.5 g/s, 45 kW, 14%, 40%, and 40% for the fuel flow rate, load bank, BA valve opening, CA valve opening, and HA bypass opening, respectively. Various candidate transfer function models are considered that differ in poles, zeros, and time delays. Parameters of the transfer function models are estimated using the outputs and corresponding PRBS inputs. The transfer function model is then validated using the data generated with a different set of PRBS input signals for the manipulated variables and the disturbances. Akaike's final prediction error criterion as shown in eq 16 is used as the criterion for model selection:

$$\text{FPE} = \det\left(\frac{1}{N}\sum_{1}^{N} \epsilon(t, \hat{\theta}_{\text{N}})\epsilon(t, \hat{\theta}_{\text{N}})^{\text{T}}\right)\left(\frac{1 + n_\theta/N}{1 - n_\theta/N}\right) \tag{16}$$

In eq 16, N is the number of values in the estimation data set, $\epsilon(t)$ is the vector or prediction errors, n_θ is the number of estimated parameters, and $\hat{\theta}_{\text{N}}$ is the vector of estimated parameters. Figures 5 and 6 show the comparison between the process (the Simulink model) and the model (the transfer function model) for the validation data set for two outputs—temperature to the plenum and temperature to the turbine.

3.2.2. Estimation of Implementation Error. The implementation error captured by the diagonal matrix M_n in eq 12 can be due to the measurement noise and other uncertainties.[26] This must therefore be estimated. For the HyPer facility, it was assumed that the implementation error would solely stem forth from the measurement data. The experimental data from the HyPer facility is used to estimate the noise similar to the work of Garcia.[37] Suppose the true value of a measured variable denoted by $\hat{y} \in \mathbb{R}^{n_y}$, then the measured data $y \in \mathbb{R}^{n_y}$ are given by

https://dx.doi.org/10.1021/acs.iecr.0c02865
Ind. Eng. Chem. Res. 2020, 59, 20058−20070

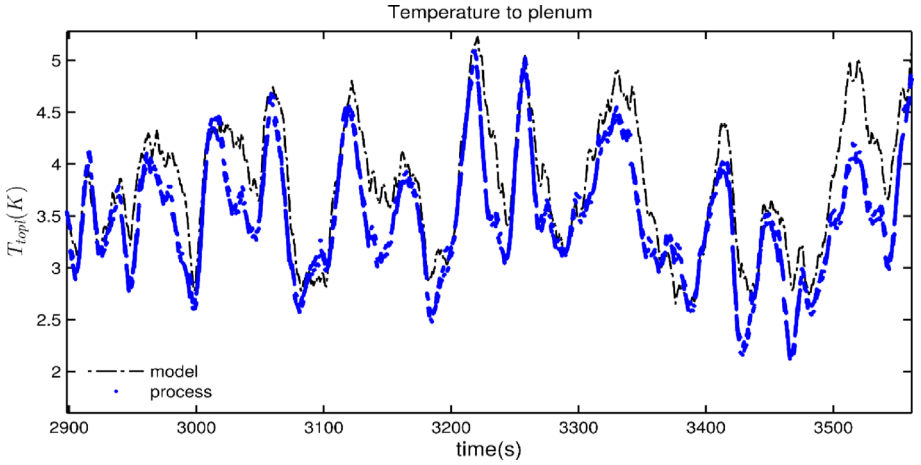

Figure 5. Comparison of model response (dash dot black) and process data (star blue) for temperature to the plenum.

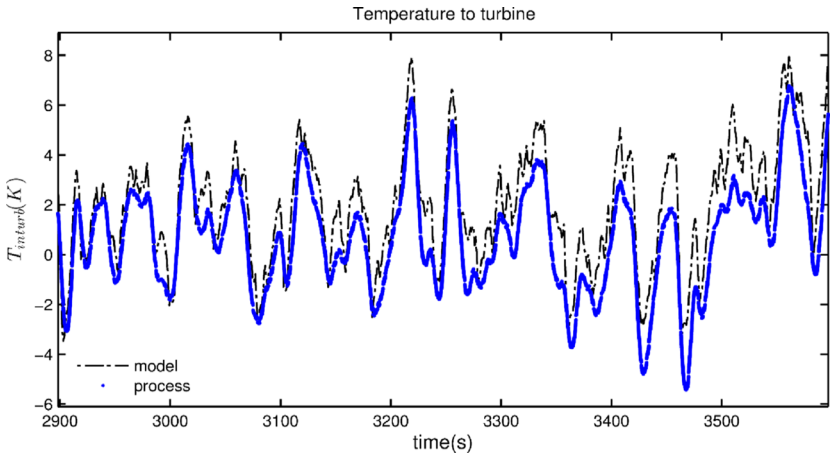

Figure 6. Comparison of model response (dash dot black) and process data (star blue) for temperature to the turbine.

$$y = \hat{y} + \varepsilon \tag{17}$$

In order to evaluate the magnitude of variance $\mathbb{E}[\varepsilon^{\mathrm{T}}\varepsilon]$, certain assumptions about the noise characteristics are necessary. For this problem, it is assumed that the noise is Gaussian and the variance of the noise is estimated from the residuals ε when the data are fit using a discretized smoothing spline.[37] Data smoothing is achieved through the minimization of the residual sum of squares (RSS) and a penalty for smoothness $P(\hat{y})$ as given by eq 18. The degree of smoothing is controlled by the parameter s. The penalty is given as the tridiagonal matrix D, which is the second order difference matrix.

$$F(\hat{y}) = \mathrm{RSS} + sP(\hat{y}) = \|y - \hat{y}\|^2 + s\,\|D\hat{y}\|^2 \tag{18}$$

Minimizing eq 18 with respect to $\hat{y}$ yields

$$(I_{\mathrm{n}} + sD^{\mathrm{T}}D)\hat{y} = H\hat{y} = y \tag{19}$$

The parameter s is chosen to minimize the generalized cross-validation (GCV) score as proposed,[38] and this is given by

$$s = \text{argmin GCV} \equiv \frac{\mathrm{RSS}/n}{1 - tr(H^{-1})/{n_{\mathrm{y}}}^2} \tag{20}$$

where the RSS is given by $\|y - \hat{y}\|^2$ in eq 18. Trace is denoted by tr. The number of samples is n. The estimated data $\hat{y}$ are obtained using discrete cosine transform (DCT); thus, the noise variance is obtained as

$$\begin{aligned}&\mathbb{E}[(y - \hat{y})^T(y - \hat{y})]\\ &= \mathbb{E}[\varepsilon^{\mathrm{T}}\varepsilon]\\ &= n_{\mathrm{y}}\sum_i \left(\frac{1}{1 + s{\lambda_{\mathrm{i}}}^2} - 1\right)^2 \mathrm{DCT}_{\mathrm{i}}^2(y)\end{aligned} \tag{21}$$

where $\lambda_{\mathrm{i}}\ \forall\ i = 1, \ldots, n_{\mathrm{y}}$, which are the eigenvalues of the matrix Λ obtained from the eigenvalues decomposition D, that is, $D = U\Lambda U^{-1}$. This algorithm is applied to the experimental data from the HyPer facility. Estimated noise variances are shown in Table 4, while comparison of smoothed data and raw data of some of the measured variables is shown in Figure 7.

3.2.3. Cost Function. The economic cost function for the HyPer facility is represented by the operating costs minus the income from selling power to the grid as shown in eq 22. The compressor work and losses in terms of equivalent electricity are denoted by $\dot{W}_{\mathrm{comp}}$ and $\dot{W}_{\mathrm{loss}}$, respectively. Electric power generated by the GT and SOFC are given by $\dot{W}_{\mathrm{elec,\ turb}}$ and $\dot{W}_{\mathrm{elec,\ FC}}$, respectively. The fuel flow denoted by $\dot{Q}$ is expressed in terms of flow of the equivalent LHV calorific value. Both the price of electricity and price of natural gas are obtained from the U.S. Energy Information Administration (EIA) http://www.eia.gov/electricity/monthly/pdf/epm.pdf. The cost of electricity is 10.07 cent/kWh. The cost of natural gas is

https://dx.doi.org/10.1021/acs.iecr.0c02865
Ind. Eng. Chem. Res. 2020, 59, 20058−20070

Table 4. Estimates of Noise Variance for Candidate CVs

s/n	candidate controlled variable		
	variable	description	noise variance
1.	$\dot{m}_{in,\ pl}$	mass flow rate to the plenum	3.9652E-10
2.	$T_{in,\ pl}$	temperature to the plenum	5.1549E-4
3.	T_{pl}	temperature in the plenum	3.1992E-3
4.	$T_{in,\ turb}$	inlet temperature to the turbine	6.0983E-3
5.	T_{pc}	temperature in the post-combustor	7.2492E-3
6.	T_{com}	temperature in the combustor	7.2492E-3
7.	ω	turbine speed	1.0E4
8.	$\dot{m}_{in,\ HX}$	mass flow rate to the heat exchanger	3.9652E-10
9.	$\dot{m}_{in,\ pc}$	mass flow rate to the postcombustor	3.9652E-10

obtained to be \$2.45/MMBtu, which translates to \$0.84 cent/kWh.

$$-J\left(\frac{\$}{h}\right) = 0.1007(\dot{W}_{comp} + \dot{W}_{loss} - \dot{W}_{elec,turb} - \dot{W}_{elec,FC}) + 0.0084\dot{Q} \quad (22)$$

It can be observed in eq 8 that the second order derivative of the cost function with respect to inputs and with respect to inputs and disturbances are needed. The cost function in eq 22 is not an explicit function of the input "u" and disturbances "d"; thus, the cost is evaluated from the data obtained from the process, and this cost is regressed to a second order quadratic function in the input space (see Table 2 for manipulated variables "u" and disturbances "d"). Therefore, the parameters of the cost function to be employed in the CV selection J_{uu}, J_{ud} are determined.

3.3. Selection of Pareto Sets with Multiagent Optimization. The optimization as defined in eq 12 was implemented on an Intel Xeon CPU E-5-1620 v2 with 32 GB RAM using the heterogeneous multiagent framework with three agents: efficient ant colony optimization, simulated annealing, and genetic algorithm. The heterogeneous multiagent optimization framework is programed in MATLAB. A framework ID is allocated to the MAOP solver that indicates which agents are to be utilized in the solution. Each agent is initialized with local parameter settings and is only accessed by the agents. Contrarily, global parameters are accessed by all the agents in the memory sharing environment. The termination criteria for the framework are the maximum global iteration MaxIter and/or the global tolerance Eps, which is the minimum allowable difference between any two consecutive solutions within a fixed number of consecutive iterations denoted as ConIter. The termination criteria for the local agents follow a similar approach. All the agents are cast into the multiagent framework with parameters as described in Table 5.

For this specific problem, the metaheuristic algorithms with three agents are found to match exactly with the results obtained using the branch and bound optimization at least for the top 20 CV sets. The metaheuristic algorithms take approximately 57 s per solution totaling 15 min, while the

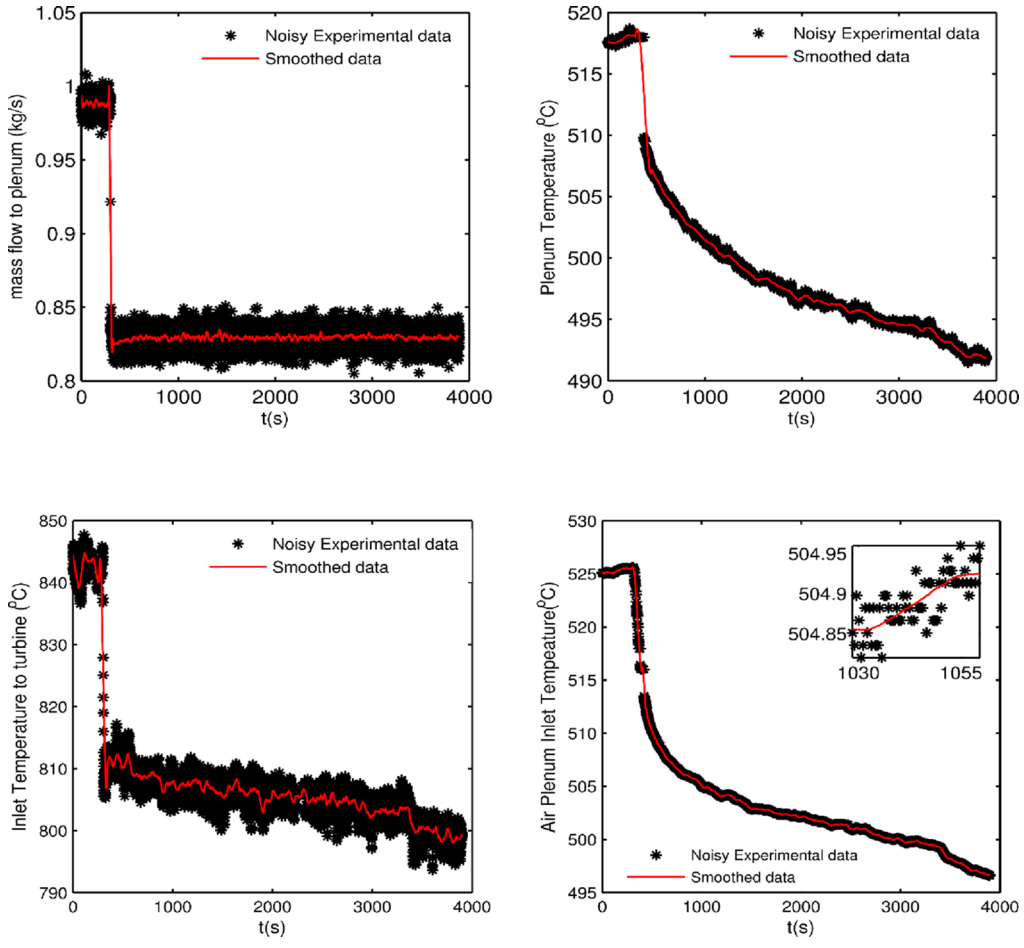

Figure 7. Comparison showing smoothed data and noisy data.

https://dx.doi.org/10.1021/acs.iecr.0c02865
Ind. Eng. Chem. Res. 2020, 59, 20058−20070

Table 5. Parameters for the Agents

	initial temperature	quenching factor	maximum success	MaxIter	maximum consecutive rejection	stop temperature
simulated annealing	1	0.9	20	200	30	1e-6
genetic algorithm	population	mutation rate	selection	MaxIter	ConIter	Eps
	100	0.0075	0.55	1000	20	1e-5
efficient ant colony	number of ants	pheromone evaporation	solution Archive	MaxIter	ConIter	Eps
	10	0.7	50	2000	10	1e-5

branch and bound optimization executes with a runtime of more than four times than the multiagent optimization framework. While for this specific problem, the savings in computational time do not appear to be large especially for an offline algorithm, it should be noted that this difference can grow up to be unacceptable. For example, if the metaheuristic algorithms take 12 h, while the branch and bound algorithm takes 2 days, it may not be acceptable. Furthermore, as the combinatorial problem grows in size, the MAOP algorithm can save considerable time as its computational expense does not grow as much like the branch and bound algorithm. For example, in one of our previous papers where a much larger combinatorial optimization problem was solved for 5.14×10^9 candidate combinations, the computational expense of the MAOP algorithm with three agents executed on an Intel Xeon CPU E-5-1620 v2 with 32GB RAM was compared with that of a nonparallelized branch and bound algorithm executed in the same desktop and a parallelized branch and bound algorithm deployed on a MATLAB-distributed computing platform with 54 workers (Bankole et al., 2019). It was observed that the MAOP resulted in about a 90% reduction in execution time in comparison with the nonparallelized branch and bound algorithm and a 23% reduction in comparison with a parallelized branch and bound algorithm.

Top 16 CV sets obtained from the multiobjective optimization are shown in Table 6. Based on these results, it

Table 6. Top 16 Pareto CV Sets

controlled variable set	controlled variable	econ($/h)	controllability (σ)
C0	1,2,5	34.75	1.00
C1	2,5,8	35.65	0.99
C2	1,3,5	36.26	0.91
C3	3,5,8	37.22	0.90
C4	2,5,9	31.46	0.76
C5	3,5,9	33.97	0.75
C6	3,5,7	81.33	0.77
C7	2,5,7	85.78	0.28
C8	1,3,6	31.61	0.76
C9	1,2,6	34.64	0.28
C10	3,6,8	37.31	0.25
C11	2,6,8	40.79	0.25
C12	3,6,9	74.44	0.32
C13	2,6,9	75.72	0.32
C14	1,5,7	162.71	0.38
C15	5,7,8	197.11	0.37

is observed that the CVs with the most self-optimizing performance are the mass flow rate to the plenum (1), the temperature in the plenum (2), and the temperature in the postcombustor (5), that is, set C0:[1,2,5]. This is because of the low expected value of the economic loss ($34.75/h) and a high minimum singular value compared with other CV sets. Therefore, it exhibits the best compromise of economics and controllability at the nominal conditions. A Pareto plot of all CV sets is given in Figure 8. The sets at the top of the table are

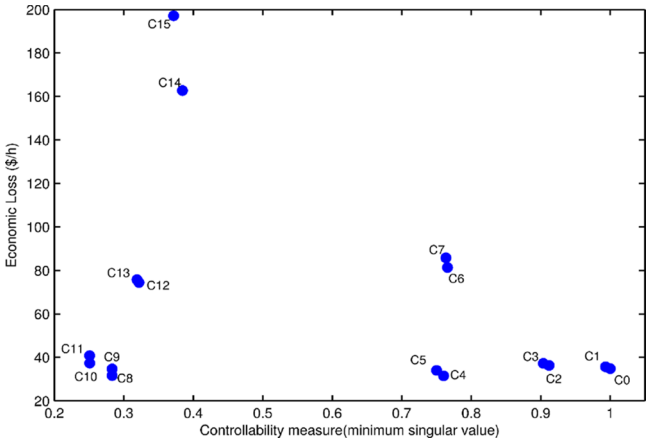

Figure 8. Pareto plots of the controlled variable selection problem.

represented in the lower right corner of Figure 8, and they represent lower economic loss and higher controllability. Contrarily, CV sets at the bottom of Table 6 are depicted toward the left portion of Figure 8. It should be noted that some CV sets such as C8−C11 that offer a great economic performance exhibit poor controllability and therefore cannot be selected.

It can be seen that all sets have some form of mass flow rate control. The control of the mass flow rate is important in the HyPer facility due to the coupled nature of the mass flow rate and power production. In addition, if the mass flow rate is not controlled, it can lead to compressor surge and stall under limiting conditions. Second, most sets include more than one temperature. Control of temperature is crucial for the HyPer facility. The turbine and the fuel cell are coupled via the exit temperature of the flue gas from the turbine; therefore, the control of temperature especially the postcombustor temperature is crucial as this drives the turbine speed. If the temperature from the postcombustor is high, this would lead to a high turbine speed, which in turn drives the compressor at higher speed as they are connected by the same shaft. Consequently, this leads to increased airflow to the fuel cell leading to an overcool. Alternatively, if the temperature to the fuel cell is rather high, this will shorten the fuel cell life span. Therefore, fluctuations in temperature are undesirable as it leads to thermal stress on the fuel cell.[4] This, therefore, imposes the need for energy sinks and sources to offset such transients; therefore, the bypass valves are highly pertinent.

3.4. Posteriori Analysis. In this section, the top results of the Pareto sets are analyzed by considering off-design conditions. This is done by changing the values of the disturbances (the electric load and the fuel flow rate) from the preset nominal conditions ranging from 80% of the nominal

https://dx.doi.org/10.1021/acs.iecr.0c02865
Ind. Eng. Chem. Res. 2020, 59, 20058−20070

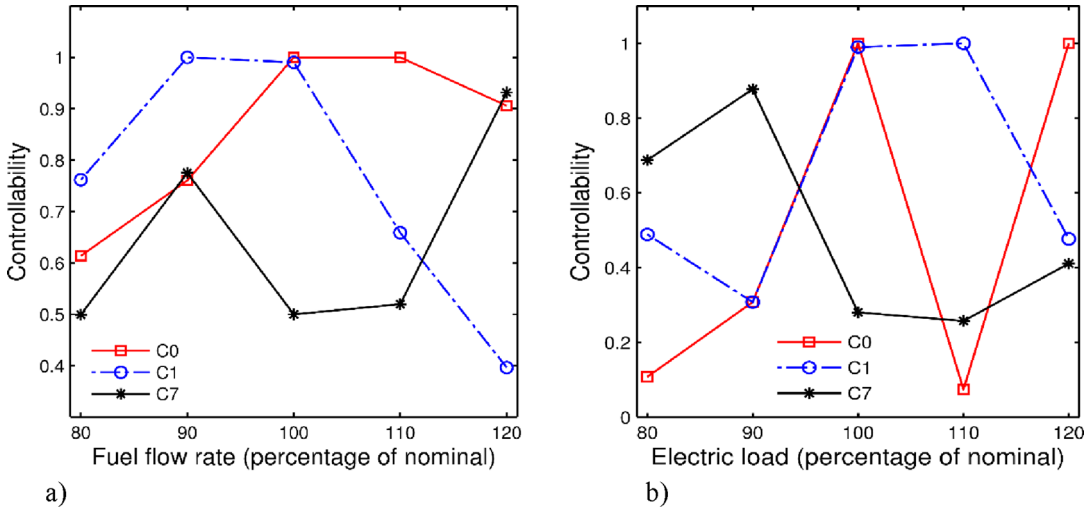

Figure 9. Controllability measure for sets C0 (square), C1 (circle), and C7 (star) at off-design points by varying (a) fuel flow rates and (b) electric loads.

value of disturbances to 120% in steps of 10%. Then, the process is run till it achieves the steady state and the gain matrices are once again identified. This process is repeated under multiple off-design conditions, and the defined controllability function $J_c(\bar{c})$ (inverse of the minimum singular value $\underline{\sigma}$ of the scaled gain matrix $\hat{G}$) is evaluated for the CV sets from the Pareto list in Table 6 (see eqs 10 and 11). For brevity, only the three sets that perform best under off-design conditions are shown in Figure 9. These are sets C0, C1, and C7. Due to the inherent nonlinearity of the process, it can be seen in Figure 9a,b that the minimum singular value is not monotonic as the disturbances vary from 80% of the nominal to 120%. It can be inferred that set C1 is the best CV set to be chosen as it has the highest average controllability of 0.706 across the disturbance variation compared with C0 and C7 with 0.675 and 0.585, respectively. This set has the best compromise between process economics and controllability, considering nominal conditions as well as off-design conditions.

4. CONCLUSIONS

In this work, a multiobjetive CV selection approach is applied to a GT-SOFC system by applying a three-stage approach—a priori analysis, CV selection, and a posteriori analysis. Several variables were prescreened off during the a priori analysis. Output data are generated from the Simulink model of the HyPer facility by applying PRBS input signals. Parameters of various candidate transfer function models are estimated using the input−output data, and the final model is selected based on Akaike's Final Prediction Error criterion. The identified model is then validated using the data generated with a different set of PRBS input signals for the manipulated variables and the disturbances. The implementation error is estimated by comparing the experimental data from the HyPer facility and assuming that it solely stems from the measurement noise; the measurement noise is Gaussian, and the measurement data follow a discretized smoothing spline. A multiagent metaheuristic platform that allows for the exploitation/combination of various agents and uses a combination of efficient ant colony, simulated annealing, and genetic algorithm is used for solving the multiobjective optimization problem. The multiagent optimization framework takes less than one-fourth of the time taken by the traditional branch and bound algorithm used for CV selection, yet it leads to solutions that have little loss in optimality compared with the solution obtained using the branch and bound algorithm. The Pareto-optimal CV sets show a high trade-off between the economic loss and controllability, but it was found that each of them contain at least one mass flow variable and typically two temperature variables with few exceptions. Top 16 Pareto-optimal CV sets are extracted for the a posteriori analysis by evaluating their performance under off-design conditions of the disturbances, namely, electric loads and fuel flow rates. It was observed that the CV set that is ranked second under nominal conditions is the preferred CV set because it shows the best compromise between process economics and controllability under both nominal and off-design conditions.

AUTHOR INFORMATION

Corresponding Author

Debangsu Bhattacharyya − *Department of Chemical and Biomedical Engineering, West Virginia University, Morgantown, West Virginia 26506, United States;* orcid.org/0000-0001-9957-7528; Phone: +1-3042939335; Email: Debangsu.Bhattacharyya@mail.wvu.edu; Fax: +1-3042934139

Authors

Temitayo Bankole − *Department of Chemical and Biomedical Engineering, West Virginia University, Morgantown, West Virginia 26506, United States; Dassault Systèmes, Wayne, Pennsylvania 19089, United States*

Paolo Pezzini − *Ames Laboratory, Ames, Iowa 50011, United States; National Energy Technology Laboratory, Morgantown, West Virginia 26507, United States*

Berhane Gebreslassie − *Vishwamitra Research Institute, Chicago, Illinois 60514, United States*

Nor Farida Harun − *National Energy Technology Laboratory, Morgantown, West Virginia 26507, United States*

David Tucker − *National Energy Technology Laboratory, Morgantown, West Virginia 26507, United States*

Urmila Diwekar − *Vishwamitra Research Institute, Chicago, Illinois 60514, United States;* orcid.org/0000-0002-0933-5865

https://dx.doi.org/10.1021/acs.iecr.0c02865
Ind. Eng. Chem. Res. 2020, 59, 20058−20070

Kenneth M. Bryden − *Ames Laboratory, Ames, Iowa 50011, United States; Iowa State University, Ames, Iowa 50011, United States*

Complete contact information is available at: https://pubs.acs.org/10.1021/acs.iecr.0c02865

Notes

The authors declare no competing financial interest.

This paper was prepared as an account of work sponsored by an agency of the U.S. Government. Neither the U.S. Government nor any agency thereof, nor any of their employees, makes any warranty, expresses, implies, or assumes any legal liability or responsibility for the accuracy, completeness, or usefulness of any information, apparatus, product, or process disclosed, or represents that its use would not infringe privately owned rights. Reference herein to any specific commercial product, process, or service by trade name, trademark, manufacturer, or otherwise does not necessarily constitute or imply its endorsement, recommendation, or favoring by the U.S. Government or any agency thereof. The views and opinions of authors expressed herein do not necessarily state or reflect those of the U.S. Government or any agency thereof.

■ ACKNOWLEDGMENTS

The work was funded by the U.S DOE through the project titled "Development of Integrated Biomimetic Framework with Intelligent Monitoring, Cognition, and Decision Capabilities for Control of Advanced Energy Plants" (Grant #: DE-FE0012451). The DOE financial support is gratefully acknowledged by the authors of this paper.

■ ADDITIONAL NOTE

[1]In absence of measurement data, measurement error can be estimated based on the expected error in the measurement technology/device.

■ REFERENCES

(1) Adams, T. A., II; Nease, J.; Tucker, D.; Barton, P. I. Energy conversion with solid oxide fuel cell systems: A review of concepts and outlooks for the short-and long-term. *Ind. Eng. Chem. Res.* **2012**, *52*, 3089−3111.

(2) Bhattacharyya, D.; Rengaswamy, R. A review of solid oxide fuel cell (SOFC) dynamic models. *Ind. Eng. Chem. Res.* **2009**, *48*, 6068−6086.

(3) Singhal, S. C.; Kendall, K. *High-temperature solid oxide fuel cells: fundamentals, design and applications*, 2003. Elsevier, Oxford UK, 293−327.

(4) Tucker, D.; Lawson, L.; Gemmen, R. *Characterization of air flow management and control in a fuel cell turbine hybrid power system using hardware simulation. ASME 2005 Power Conference*, 2005. American Society of Mechanical Engineers, 959−967.

(5) Winkler, W.; Nehter, P.; Williams, M. C.; Tucker, D.; Gemmen, R. General fuel cell hybrid synergies and hybrid system testing status. *J. Power Sources* **2006**, *159*, 656−666.

(6) Balas, G. J. Flight control law design: An industry perspective. *Eur. J. Control* **2003**, *9*, 207−226.

(7) van de Wal, M.; de Jager, B. A review of methods for input/output selection. *Automatica* **2001**, *37*, 487−510.

(8) Larsson, T.; Skogestad, S. Plantwide control-A review and a new design procedure. *Model. Identif. Control* **2000**, *21*, 209.

(9) Jäschke, J.; Cao, Y.; Kariwala, V. Self-optimizing control−A survey. *Annu. Rev. Control* **2017**, *43*, 199−223.

(10) Murthy Konda, N. V. S. N.; Rangaiah, G. P.; Krishnaswamy, P. R. Plantwide control of industrial processes: An integrated framework of simulation and heuristics. *Ind. Eng. Chem. Res.* **2005**, *44*, 8300−8313.

(11) Fisher, W. R.; Doherty, M. F.; Douglas, J. M. Steady-state control as a prelude to dynamic control. *Chem. Eng. Res. Design* **1985**, *63*, 353−357.

(12) Skogestad, S. Plantwide control: The search for the self-optimizing control structure. *J. Process Control* **2000**, *10*, 487−507.

(13) Jones, D.; Bhattacharyya, D.; Turton, R.; Zitney, S. E. Plant-wide control system design: Primary controlled variable selection. *Comput. Chem. Eng.* **2014**, *71*, 220−234.

(14) Halvorsen, I. J.; Skogestad, S.; Morud, J. C.; Alstad, V. Optimal selection of controlled variables. *Ind. Eng. Chem. Res.* **2003**, *42*, 3273−3284.

(15) Cao, Y.; Kariwala, V. Bidirectional branch and bound for controlled variable selection: Part I. Principles and minimum singular value criterion. *Comput. Chem. Eng.* **2008**, *32*, 2306−2319.

(16) Kariwala, V.; Cao, Y. Bidirectional branch and bound for controlled variable selection. Part II: Exact local method for self-optimizing control. *Comput. Chem. Eng.* **2009**, *33*, 1402−1412.

(17) Kariwala, V.; Cao, Y. Bidirectional branch and bound for controlled variable selection part iii: local average loss minimization. *IEEE Trans. Ind. Inform.* **2010**, *6*, 54−61.

(18) Gebreslassie, B. H.; Diwekar, U. M. *Multi-agent Optimization Framework (MAOP) for Large Scale Process System Engineering Optimization Problems*. AIChE Annual Meeting 2015 Salt Lake

(19) Bankole, T.; Bhattacharyya, D.; Gebreslassie, B.; Diwekar, U. A biomimetic approach to fast selection of optimal controlled variables using multi-agent algorithms and a decomposition approach. *Chem. Eng. Sci.* **2019**, *203*, 475−488.

(20) Smith, T. P.; Haynes, C. L.; Wepfer, W. J.; Tucker, D.; Liese, E. A. Hardware-based simulation of a fuel cell turbine hybrid response to imposed fuel cell load transients. *ASME 2006 International Mechanical Engineering Congress and Exposition*, 2006. American Society of Mechanical Engineers, 319−328.

(21) Bankole, T.; Bhattacharyya, D. Exploiting connectivity structures for decomposing process plants. *J. Process Control* **2018**, *71*, 116−129.

(22) Bankole, T.; Pezzini, P.; Tucker, D.; Bryden, K.; Bhattacharyya, D. Optimal Controlled Variable Selection for Cyber-Physical Systems. In *ASME 2018 Power Conference collocated with the ASME 2018 12th International Conference on Energy Sustainability and the ASME 2018 Nuclear Forum*, 2018. American Society of Mechanical Engineers Digital Collection.

(23) Shi, J.; Wan, J.; Yan, H.; Suo, H. A survey of cyber-physical systems. *Wireless Communications and Signal Processing (WCSP), 2011 International Conference on*, 2011. IEEE, 1−6.

(24) Zhao, J.; Wen, F.; Xue, Y.; Li, X.; Dong, Z. Cyber physical power systems: architecture, implementation techniques and challenges. *Dianli Xitong Zidonghua/Automation Electr. Power Syst.* **2010**, *34*, 1−7.

(25) Jones, D.; Bhattacharyya, D.; Turton, R.; Zitney, S. E. Plant-wide control system design: Secondary controlled variable selection. *Comput. Chem. Eng.* **2014**, *71*, 253−262.

(26) Kariwala, V.; Cao, Y.; Janardhanan, S. Local self-optimizing control with average loss minimization. *Ind. Eng. Chem. Res.* **2008**, *47*, 1150−1158.

(27) Bankole, T.; Bhattacharyya, D. Nonlinear optimal control structure design, *AIChE Annual Meeting, October 28-November 2, 2018, Pittsburgh, PA*, 2018.

(28) Gebreslassie, B. H.; Diwekar, U. M. Efficient ant colony optimization for computer aided molecular design: case study solvent selection problem. *Comput. Chem. Eng.* **2015**, *78*, 1−9.

(29) Kim, K.-J.; Diwekar, U. M. Hammersley stochastic annealing: efficiency improvement for combinatorial optimization under uncertainty. *IIE Trans.* **2002**, *34*, 761−777.

(30) Xu, W.; Diwekar, U. M. Improved genetic algorithms for deterministic optimization and optimization under uncertainty. Part II. Solvent selection under uncertainty. *Ind. Eng. Chem. Res.* **2005**, *44*, 7138−7146.

(31) Siirola, J. D.; Hauan, S.; Westerberg, A. W. Toward agent-based process systems engineering: Proposed framework and application to non-convex optimization. *Comput. Chem. Eng.* **2003**, *27*, 1801−1811.
(32) Gebreslassie, B. H.; Diwekar, U. M. Homogenous multi-agent optimization for process systems engineering problems with a case study of computer aided molecular design. *Chem. Eng. Sci.* **2016**, *159*, 194−206.
(33) Tsai, A.; Banta, L.; Tucker, D.; Gemmen, R. Multivariable robust control of a simulated hybrid solid oxide fuel cell gas turbine plant. *J. Fuel Cell Sci. Technol.* **2010**, *7*, No. 041008.
(34) Tucker, D.; Shelton, M.; Manivannan, A. The role of solid oxide fuel cells in advanced hybrid power systems of the future. *Electrochem. Soc. Interface* **2009**, *18*, 45.
(35) Tucker, D.; Smith, T.; Lawson, L. *Characterization of Bypass Control Methods in a Coal-Based Fuel Cell Turbine Hybrid. Irvine, CA, Paper No. ICEPAG2006-24008*, 2006.
(36) Gaikwad, S.; Rivera, D. Control-relevant input signal design for multivariable system identification: Application to high-purity distillation. *IFAC World Congress*, 1996. Citeseer.
(37) Garcia, D. Robust smoothing of gridded data in one and higher dimensions with missing values. *Comput. Stat. Data Anal.* **2010**, *54*, 1167−1178.
(38) Craven, P.; Wahba, G. Smoothing noisy data with spline functions. *Numer. Math.* **1978**, *31*, 377−403.

https://dx.doi.org/10.1021/acs.iecr.0c02865
Ind. Eng. Chem. Res. 2020, 59, 20058−20070